Density Functional Theory Study of Rutile SiO_2 Stishovite: An Electron Pair Description of Bulk and Surface Properties

by

Thomas Muscenti

Thesis submitted to the Chemical Engineering faculty of Virginia Polytechnic Institute and State University in partial fulfillment of the requirements for a degree of

Masters of Science

in

Chemical Engineering

Approved by:

Dr. D. F. Cox, Chair

Dr. G.V. Gibbs

Dr. S.T. Oyama

October 8, 2004

Blacksburg, Virginia

Keywords: stishovite, surface, hydrogen fluoride, adsorption, electron localization

Density Functional Theory Study of Rutile SiO_2 Stishovite: An Electron Pair Description of Bulk and Surface Properties

by

Thomas Muscenti

ABSTRACT

The bulk structure and the nonpolar, stoichiometric (110) surface of stishovite, rutile structure type SiO_2, has been studied using a first principles, density functional method. The geometric and electronic structure, including the density of states, charge density, and electron localization function for both the bulk and the surface have been examined. The electron pair properties of both bulk and surface-layer atoms were found to be similar to molecular analogs. The analogs allowed for the description of surface electronic structure using simple molecular models. The adsorption of hydrogen fluoride was studied on the (110) surface. The geometry optimized and electronic structure have been found for various initial geometries. Relaxed structures of certain initial geometries give dissociated hydrogen fluoride upon geometry optimization.

Table of Contents

List of Figures

List of Tables

ACKNOWLEDGEMENTS

I would like to thank Dr. David F. Cox for his continual instruction, guidance, and support throughout my studies and research. I also appreciate his help and patience with my evolution as a technical writer. His candid comments and questions helped develop my writing and thinking skills.

I am grateful to my graduate committee: Dr. Gerald V. Gibbs for sharing his knowledge of the silicon-oxygen bond, and Dr. S. Ted Oyama for his instruction in graduate courses and challenging questions inside and outside the classroom.

I would like to thank the faculty and staff at Virginia Tech for all their help and my friends for making my time in Blacksburg enjoyable and golf-filled.

I couldn't be where I am today without the love and support of my family, especially my parents. The wonderful examples they set have helped guide my life.

Finally, I give my unending appreciation and admiration to my beloved wife Molly. She has sacrificed much and has always believed in me. I cannot imagine a better person with which to share my life.

Chapter 1 - Introduction

1. Introduction

Extensive research has been done on rutile structure type oxides, such as SnO_2 and TiO_2, both experimentally and theoretically. This study focuses on another rutile structure type – stishovite, SiO_2. Unlike other silica polymorphs, stishovite is unique in the fact that it has a 6:3 coordination sphere with six-coordinate silicon and three-coordinate oxygen, compared to the more common 4:2 coordination with four-coordinate silicon and two-coordinate oxygen. Study of this unique configuration will further the understanding of the Si-O bond, which is of crystal chemical and geophysical interest. The formation of stishovite at high pressures suggests that it may be a predominant phase in silica-rich regimes lower in the Earth's mantle.

Using the density functional theory method and the VASP code, the electronic and geometric structure of stishovite and its (110) surface have been studied. The band structure and electron pair features (bonding and lone pair) of both the bulk structure and the (110) surface have been compared to other rutile structure types and their respective (110) surfaces in an effort to establish the nature of such surfaces. This study has established that the properties of the (110) surface of stishovite are similar to those observed for other rutile structure type oxides. However, the model used to understand this similarity is based on electron pairs and molecular analogs. This simple model has successfully predicted characteristics of the (110) surface of stishovite, and can be extended to describe other rutile structure types.

Stishovite is the most insoluble silica polymorph with respect to hydrogen fluoride etching. To understand its instability, the adsorption of hydrogen fluoride has

been examined in a theoretical study to probe the nature of the adsorption sites on the (110) surface of stishovite. This study of the interaction between the (110) surface of stishovite and hydrogen fluoride can be used for comparison to other silica polymorphs.

1.1 Stishovite

Stishovite is a high-pressure silica polymorph that crystallizes with the rutile structure. It was first synthesized at high temperature and pressure by Stishov and Popova in 1961 [1] and discovered naturally at the impact site at Meteor Crater, AZ, in 1962 [2]. The lattice parameters are a = 4.177 Å and c = 2.665 Å [3], with 2 formula units per unit cell.

Among the rutile crystal structures, the (110) surface had been studied for TiO_2 [4] and SnO_2 [5-8]. There have been several studies into the bulk electronic structure of stishovite [9-12], however, the (110) surface of stishovite has not yet to be studied nor have there been comparisons to other rutile structure type (110) oxide surfaces.

1.2 Methods

The calculations were completed using the Vienna Ab-initio Simulation Package (VASP) code [13-15], a first principles, density functional method that uses a plane wave basis set and periodic boundary conditions. The electronic structure is built with Vanderbilt ultra-soft pseudopotentials (US-PP) [16], which only explicitly represent valence electrons. The electron exchange and correlation are accounted for using the

Generalized Gradient Approximation (GGA) [17,18]. The pseudopotentials treat oxygen 2s and 2p levels as valence states and silicon 3s and 3p levels as valence states.

The basis set includes plane waves with kinetic energy lower than a specified cut-off energy, E_{cut}. For all calculations a value of 495 eV was used. The bulk and surface were optimized using the full space group symmetry, while total energy and adsorption geometry optimization calculations were performed using C1 point symmetry to allow for any possible (symmetric or unsymmetric) relaxation to a lower energy. The k-point sampling was generated using a Monkhorst-Pack scheme [19] and a [3 x 3 x 3] grid that generated 8 k-points (with full symmetry) and 14 k-points (with C1 symmetry). The zero pressure minimum energy volume was found for the bulk cell by varying both the cell parameters and atom positions. After the minimum energy structure was found, the cell parameters parallel to the surface were fixed at the bulk values for all subsequent surface and adsorption geometry optimization and total energy calculations.

The unit cell used for all the calculations contains 48 atoms and is arranged with four stoichiometric units along the [110] direction, each consisting of three atomic planes: a plane containing silicon and oxygen sandwiched between planes containing only oxygen, so the sequence of planes is O_2-Si_4O_4-O_2-O_2-Si_4O_4-O_2 etc. The slab used has been found to be sufficient size for the (110) surfaces of SnO_2 [5-8] and TiO_2 [4]. To create the surface, a 10 Å vacuum gap was introduced in the [110] direction. The surface energy as a function of vacuum width was tested and converged to within 0.02 eV with a 5 Å vacuum gap.

To obtain the spd- and site projected wave function character for each band, the wave functions were projected onto the spherical harmonics centered on each atom. The values

are non-zero within a given radius for each atom. The radii selected for the oxygen, silicon, hydrogen, and fluorine are 1.36, 0.93, 0.30, and 0.71 Å, respectively. The silicon and oxygen radii are proportional to those obtained by the bond critical point derivations from the electron density distribution determined in single crystal synchotron X-ray experiments by Kirfel, *et al*. [3] and were scaled so the sum of the volumes corresponding to all the silicon and oxygen spheres matched the total volume of the 48-atom bulk cell. Using the radii, the electronic charge per atom can be determined via integration of the charge density over the radius of the atoms. The shortcoming of this method is an undercount of electrons due to the excluded volume arising from filling the cell with spheres. In addition, the radii of the atoms overlap, so there is a slight overcount of electrons along the Si-O bond. The net result, however, is an overall undercount of the total number of electrons. The number of electrons counted for the bulk unit cell is 247.97 for this method, less than the 256 electrons in the 48 atom cell.

The electron localization function (ELF) has been used since its definition by Becke and Edgecombe [20] to determine qualitatively the location of paired electrons. It has not only been extensively used as a tool to explain spatial electron distribution around atoms, molecules, clusters, and solids [21], but also to describe qualitatively the polarity of chemical bonds, lone pairs, and structure according to the valence shell electron pair repulsion (VSEPR) theory [21]. This tool has been used previously to understand electronic structure of many silica polymorphs, including stishovite [22,23]. The ELF equation (Eq. 1) is seen below.

(1) $$ELF = \left\{1 + \left[\frac{C\left(\vec{r}\right)}{C_h\left(\rho\left(\vec{r}\right)\right)}\right]^2\right\}^{-1}$$

where

(2) $$C\left(\vec{r}\right) = \frac{1}{2}\sum_i n_i \left|\nabla \varphi_i\right|^2 - \frac{1}{8}\frac{\left|\nabla\rho\right|^2}{\rho}$$ and

(3) $$\rho = \sum_i n_i \left|\varphi_i^{\,2}\right|$$

The function $C\left(\vec{r}\right)$ measures the difference between the kinetic energy of the actual system and the kinetic energy of the system without the Pauli exclusion principle, where φ_i is the wave function. The value of $C\left(\vec{r}\right)$ is inversely proportional to the degree of localization: the higher the localization, the smaller the value. $C_h\left(\vec{r}\right)$ represents the value of the function $C\left(\vec{r}\right)$ for a homogeneous electron gas (which varies as $\rho^{5/3}$), which is used as a reference. The arbitrary scale (from $0 \rightarrow 1$) has a maximum value where electron pairs (bonding and lone) are most likely to be found. The ELF has a value of 0.5 for a homogeneous electron gas.

Chapter 2 – Bulk and Surface Comparison

2.1 Bulk

2.1.1 Geometric Structure

The geometry optimized 48 atom supercell of bulk stishovite is displayed in Figure 2.1, where the Si:O 6:3 coordination can be seen. The forces on the individual atoms for the relaxed structures were less than 0.05 eV/Å. The SiO_6 octahedron is distorted, with bond lengths being 1.817 Å and 1.793 Å for the axial and equatorial Si-O bonds, respectively. These results compare favorably with the experimental bond lengths of 1.813 Å and 1.756 [24]. The oxygen is three coordinate, with three Si-O bonds lying in the same plane. A pair of bond angles are 130.1º and the third is 99.8º. These also compare favorably to the values (130.6º and 99.2º) reported by Ross, *et al*. [24] from single crystal X-ray diffraction.

2.1.2 Electronic Structure and Density of States

The number of valence electrons attributed to bulk silicon and oxygen are 0.9 and 7.4, respectively. This corresponds to charges of +3.1 for silicon and –1.4 for oxygen, which is consistent with the results from atomic basin calculations of Kirfel, *et al*. [3]. The non-zero net charge is another indication of the imperfection of the site projection method. Due to the symmetry in the calculation, the electron count is identical for all silicon and oxygen atoms in bulk stishovite.

The total density of states (DOS) for bulk stishovite and partial density of states (PDOS) for oxygen and silicon are seen in Figure 2.2. The 0 eV position in all figures is

Figure 2.1. 48 atom Supercell of Bulk Stishovite. Large red spheres are oxygen, small blue spheres are silicon.

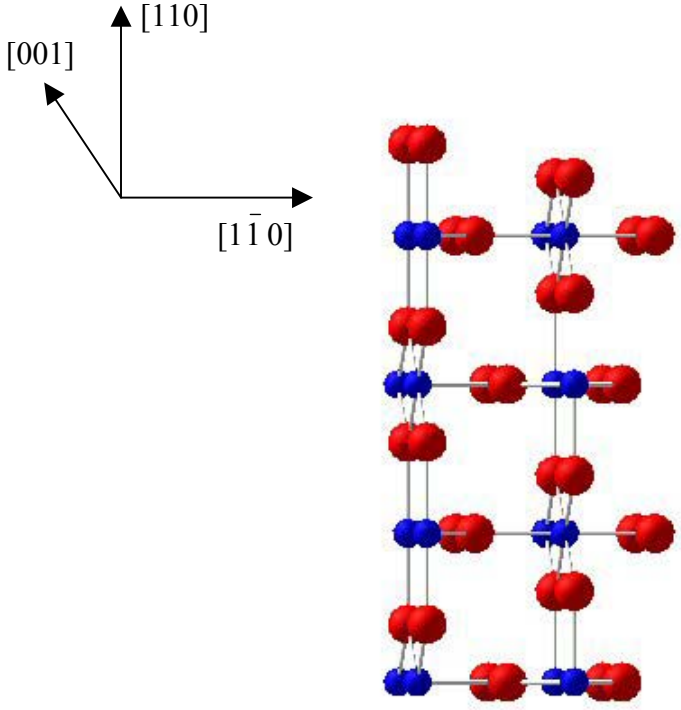

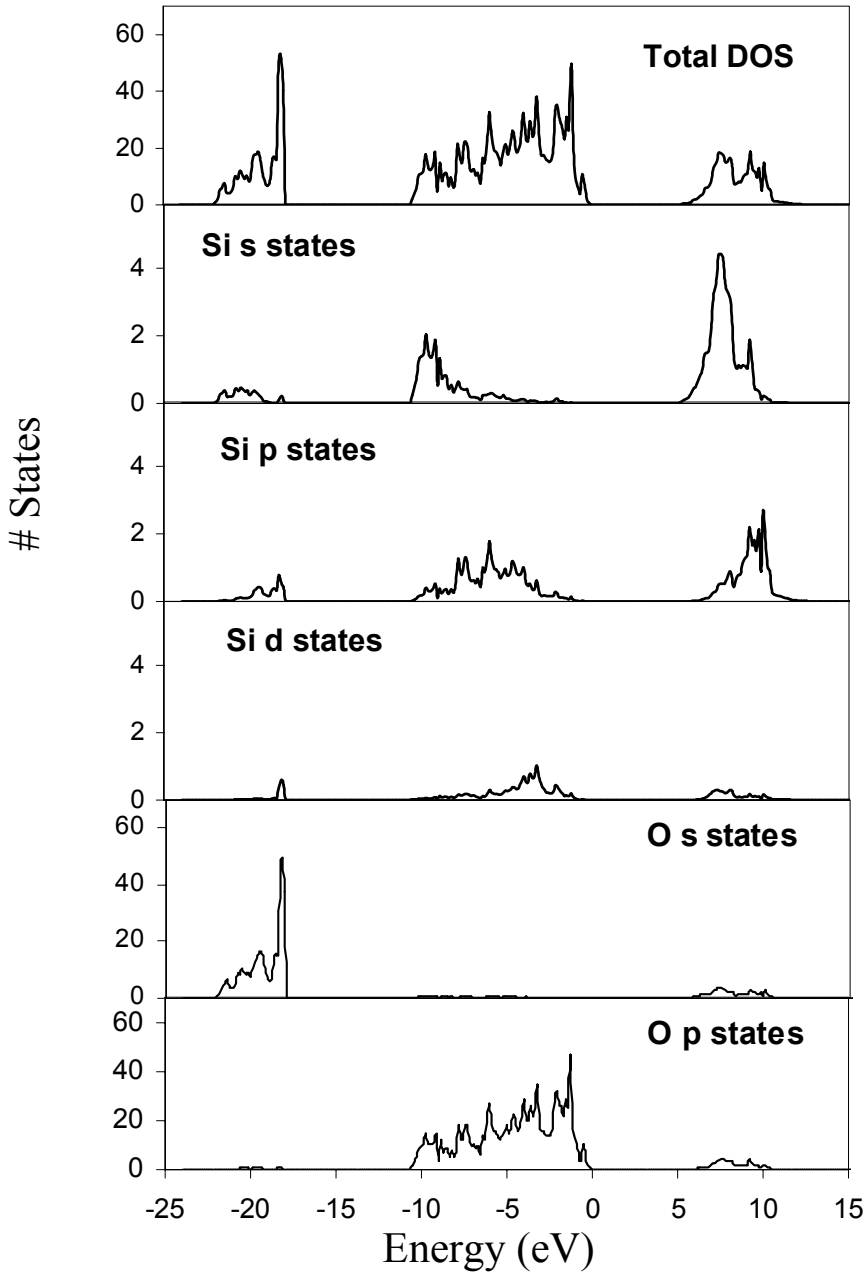

Figure 2.2. The calculated total density of states (DOS) for the bulk and partial density of states (PDOS) for oxygen and silicon. 0 eV is defined as the Fermi level.

defined as the Fermi level. Inspection of the figure shows three distinct band regions: a semi-core level, a valence level, and a conduction level.

The lower, semi-core region from –22.0 eV to –17.9 eV is predominately O(2s) in character, with any features due to silicon due to the of the overlap of the assigned atomic radii, which would project oxygen electron density onto silicon. The valence band is 10.6 eV wide and consists of bonding and nonbonding states. The lower region of the band, –10.6 eV to –8.0 eV, is composed of Si(s) and O(2p) bonding states. The middle region of the band, -8 eV to –3.6 eV, is composed of Si(p) and O(2p) bonding states. The upper region of the band, -3.6 eV to 0 eV, is composed of O(2p) states. The conduction band is predominately composed of Si states and the conduction band minimum has mostly s state composition. The silicon d states only contribute slightly to the valence band. The features (both relative location and peak shapes) of the site-projected PDOS for the individual atoms agree with the localized density of states calculated with the pseudopotential and linearized augmented plane wave methods by Alvarez, *et al*. [9].

The site projected wave function character was examined at the Γ point, however, other points in reciprocal space reproduced the same qualitative results. The highest occupied band was found to consist of nonbonding O(2p) states perpendicular to the bonding plane defined by the Si-O bonds.

The direct band gap measured at the Γ point was 4.9 eV, which is smaller than the experimental value of 5.7 eV [11], and agrees well with other theoretical calculations using both pseudopotential (5.3 eV) and linear, augmented plane wave (5.5 eV) methods [**9**].

2.1.3 ELF and Charge Density Maps

The electron localization function shows features that can be ascribed to domains of bonding and lone pairs of electrons. Figure 2.3 shows two ELF values: the first shows a distribution around the oxygen atom at an ELF value of 0.835, but when the ELF is increased to a value of 0.855, features along the Si-O bond axis, which represent bonding electron pairs, and two features above and below the plane of the Si-O bonds, which resemble an electron lone pair in the p orbital perpendicular to the bonding plane, are seen to remain. The bond pairs are located closer to the oxygen, which is an indication of the polar nature of these bonds. The lone pair features described by the ELF match the valence band features for oxygen p orbitals. These features would best describe an oxygen atom in the sp^2 hybrid state.

The charge density isosurface shows the same lone-pair features as the ELF. Figure 2.3 shows the charge density isosurface at a value of 6.84 $e^-/Å^3$, which shows features above and below the bonding plane that are seen in the ELF.

2.2 Surface

2.2.1 Relaxed Geometry and Energetics

To make a nonpolar stoichiometric surface, the bulk cell was cleaved in a manner to retain a row of 2-coordinate bridging oxygen atoms on each side of the slab. A vacuum layer of 10 Å was introduced in the [110] direction. This type of termination results in five distinct surface atoms per surface unit cell: two five-coordinate silicons, two six-coordinate silicons, four three-coordinate in-plane oxygens, two two-coordinate bridging, and two three-coordinate sub-bridging oxygens. The stoichiometric surface

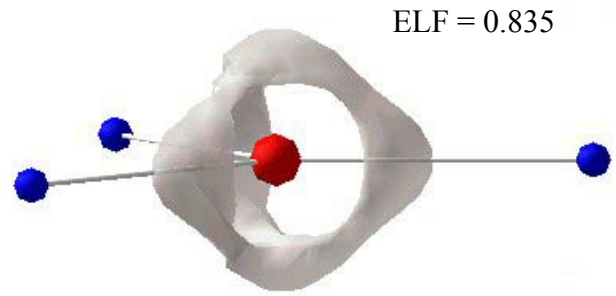

A

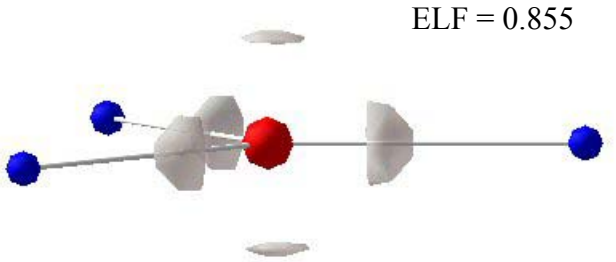

B

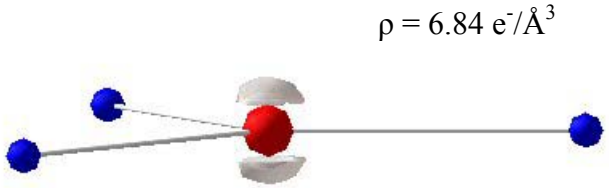

C

Figure 2.3. (a): Oxygen atom ELF value 0.835. (b): Oxygen atom ELF value 0.855. (c): charge density isosurface (6.84 $e^-/Å^3$). The large red spheres are oxygen and the small blue spheres are silicon. As the ELF value is increased, the singular feature breaks into bonding pair features along the Si-O bonds and lone-pair like features above and below the bonding plane. The lone-pair features can also be seen in the charge density isosurface.

units consist of three atomic planes: (bridging oxygen) - (five-and six-fold silicon and in-plane oxygen) – (sub-bridging oxygen) in the same (O_2-Si_4O_4-O_2) units as the bulk. The labeled surface atoms are shown in Figure 2.4.

The surface relaxations are shown in Table 2.1 and are shown in a side by side comparison with the bulk terminated surface in Figure 2.4. The forces on the individual atoms for the relaxed structures were less than 0.05eV/Å. The relative displacements (on the order of 0.1-0.3 Å) are similar to those predicted for other rutile structure type (110) surfaces, such as TiO_2 [4] and SnO_2 [5-8]. The 5-coordinate silicons relax into the surface, while all other atoms relax outward. The axial bond in the 5-fold silicon is now shorter than the equatorial bonds, while the opposite is true for the bulk structure. The only difference between TiO_2 and stishovite is the direction for bridging oxygen displacement, which is inward for TiO_2. The relaxation is primarily perpendicular to the surface, but the in-plane oxygen atoms do relax (0.06 Å) laterally in the $[1\bar{1}0]$ toward the five-fold silicon.

The surface relaxation shortens the bond length between the bridging oxygen atoms and the six-fold silicon by about 6%, a decrease from 1.793 Å in the bulk to 1.684 Å. The bond from the six-fold silicon to the sub-bridging oxygen increases 6%, from 1.817 Å in the bulk to 1.926 Å. The bond length from the five-fold silicon to the oxygen beneath it also decreases by 7%, from 1.817 Å in the bulk to 1.692 Å. With the relaxation, the Si-O-Si bond angle between bridging atoms increases to 109.0° (from 99.8° in the bulk). Due to the surface relaxation, the silicon - in-plane oxygen bond lengths change, with the long Si-O bond (1.817 Å in the bulk) stretching (1.877 Å) and

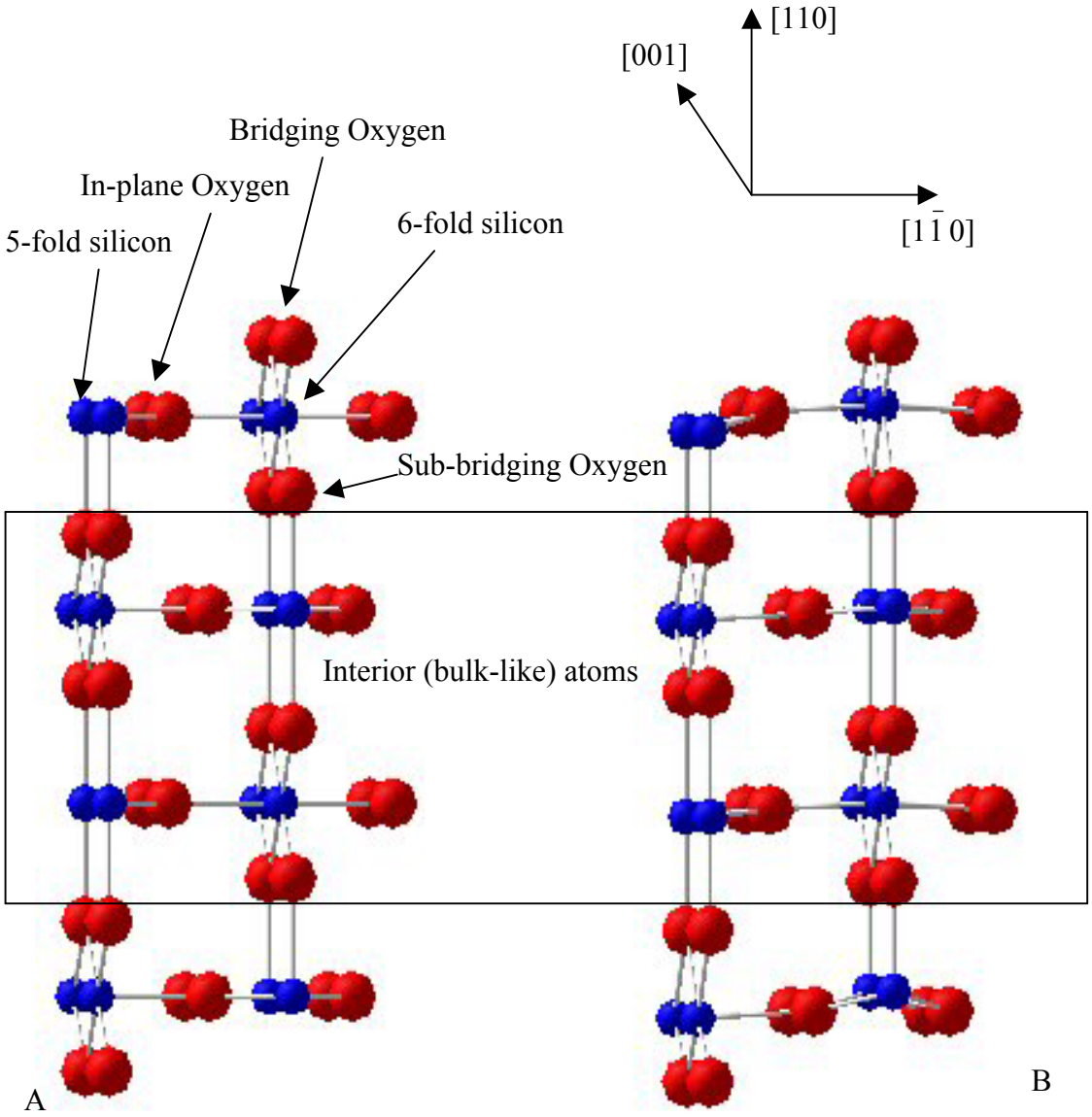

Figure 2.4. Bulk terminated (a) and relaxed (b) structures of the (110) surface. Surface atoms created by making (110) surface are shown in the relaxed surface. The large red spheres are oxygen, the small blue spheres are silicon.

Atom Type	Surface Relaxation (Å)		
	[110] direction	[$1\bar{1}0$] direction	[001] direction
5-fold Silicon	-0.15	0.00	0.00
6-fold Silicon	0.26	0.00	0.00
Sub-bridging Oxygen	0.06	0.00	0.00
In-plane Oxygen	0.15	0.06	0.00
Bridging Oxygen	0.08	0.00	0.00

Table 2.1. Surface relaxation distances and directions for surface atoms. For the [110] direction, negative values are relaxation into the surface, positive values are out of the surface. For the relaxation in the [$1\bar{1}0$] direction, positive values indicate a relaxation toward the 5-fold silicon.

the short Si-O bonds (1.793 Å in the bulk) shrinking (1.782 Å). The bond lengths between the in-plane oxygen and the unsaturated silicon decrease, while the bonds with the saturated silicon increase. Additionally, the Si-O bonds for the in-plane oxygen are no longer coplanar. The bond lengths for the unsaturated surface atoms (bridging oxygen and 5-fold silicon) decrease, while the six-fold silicon bonds to the sub-bridging oxygen increase. The percentage increase/decrease is slightly larger than those reported for SnO_2 [5].

The surface energy for the unrelaxed surface was calculated to be 2.29 J/m^2, while relaxing the surface decreases the energy to 1.13 J/m^2. The surface energy for the relaxed surface is similar to those calculated for SnO_2 (ranging from 1.0-1.4 J/m^2) [5-7] and TiO_2 [4] (0.8 J/m^2) (110) surfaces.

2.2.2 Density of States

The DOS for the relaxed surface (Figure 2.5) is similar to that of the bulk DOS, with a few important distinctions. Firstly, there are surface states split off from top of the O(2s) semi-core states, labeled A in Figure 2.5. Secondly, there are surface states at the top of the valence band, labeled B. The final difference is a reduction in the direct band gap at the Γ point, from 4.9 eV in the bulk to 3.6 eV for the relaxed surface. The reduction seems to arise from a combination of surface states at the valence band maximum (VBM) and in the band gap at the conduction band minimum (CBM), labeled C. Similar surface states near the O(2s) core, CBM, and VBM were found for the SnO_2 (110) surface DOS [6].

Figure 2.5. Total density of states for the relaxed (110) surface (top) and bulk (bottom). 0 eV is defined as the Fermi level. Surface states are seen (A) split from the semi-core states (near -17 eV) (B) at the top of the valence band (near 0 eV) and (C) in the bulk band gap region (near 4 eV).

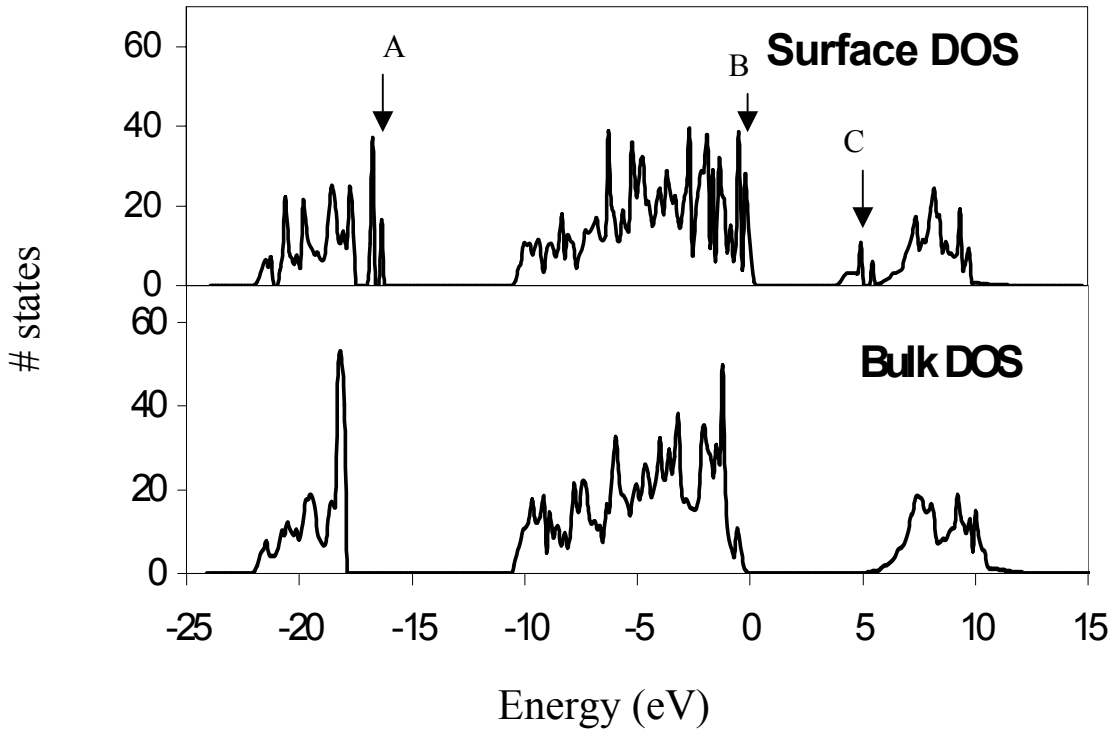

Introducing a surface changes the electronic structure of most of the atoms in the top stoichiometric surface unit (5-fold silicon, in-plane oxygen, bridging oxygen, and sub-bridging oxygen), while leaving the other bulk-like atoms unchanged. The atoms in the first stoichiometric surface unit, except for the six-fold silicon, show marked changes in the PDOS compared to the same atoms in the bulk, while the interior stoichiometric unit atoms retain more bulk-like PDOS. The PDOS for the atoms associated with the surface states are seen in Figure 2.6, along with the PDOS for the same atoms in the bulk for comparison.

To determine the character of the surface states, the partial charges of each atom type were summed over all bands within the energy range corresponding to the surface states and all k-points. The right-hand side of Figure 2.6 shows the atoms contributing to the surface states split off the O(2s) semi-core states and VBM surface states. The O(2s) surface states have a composition of 74% bridging oxygen s states, with the rest sub-bridging oxygen s states. The states at the top of the valence band (from -0.4 eV to 0 eV) are primarily (80%) composed of bridging oxygen p orbital states, which have projections along both the $[1\bar{1}0]$ and [110] directions. The remaining portion of the states is composed of in-plane and sub-bridging oxygen p states. The in-plane oxygen states are in the [110] direction, while the sub-bridging oxygen states are in the $[1\bar{1}0]$ direction (perpendicular to the bonding plane). Because the in-plane oxygen states are directed into the vacuum and there is no silicon contribution to the band, they can be described as a non-bonding electron lone pair extending into the vacuum. The left-hand side of Figure 2.6 shows the atoms contributing to the CBM surface states. The conduction band

Figure 2.6. Atomic PDOS for selected surface atoms. The solid line represents the surface atom PDOS for the relaxed surface, while the dotted line represents the PDOS for the same atom in the bulk. The surface states near the O(s) semi-core (A) and valence band maximum (B) can be seen in the PDOS of the bridging and sub-bridging oxygen. The surface states in the band gap (C) can be seen in the 5-fold silicon and the in-plane oxygen PDOS. 0 eV is defined as the Fermi level.

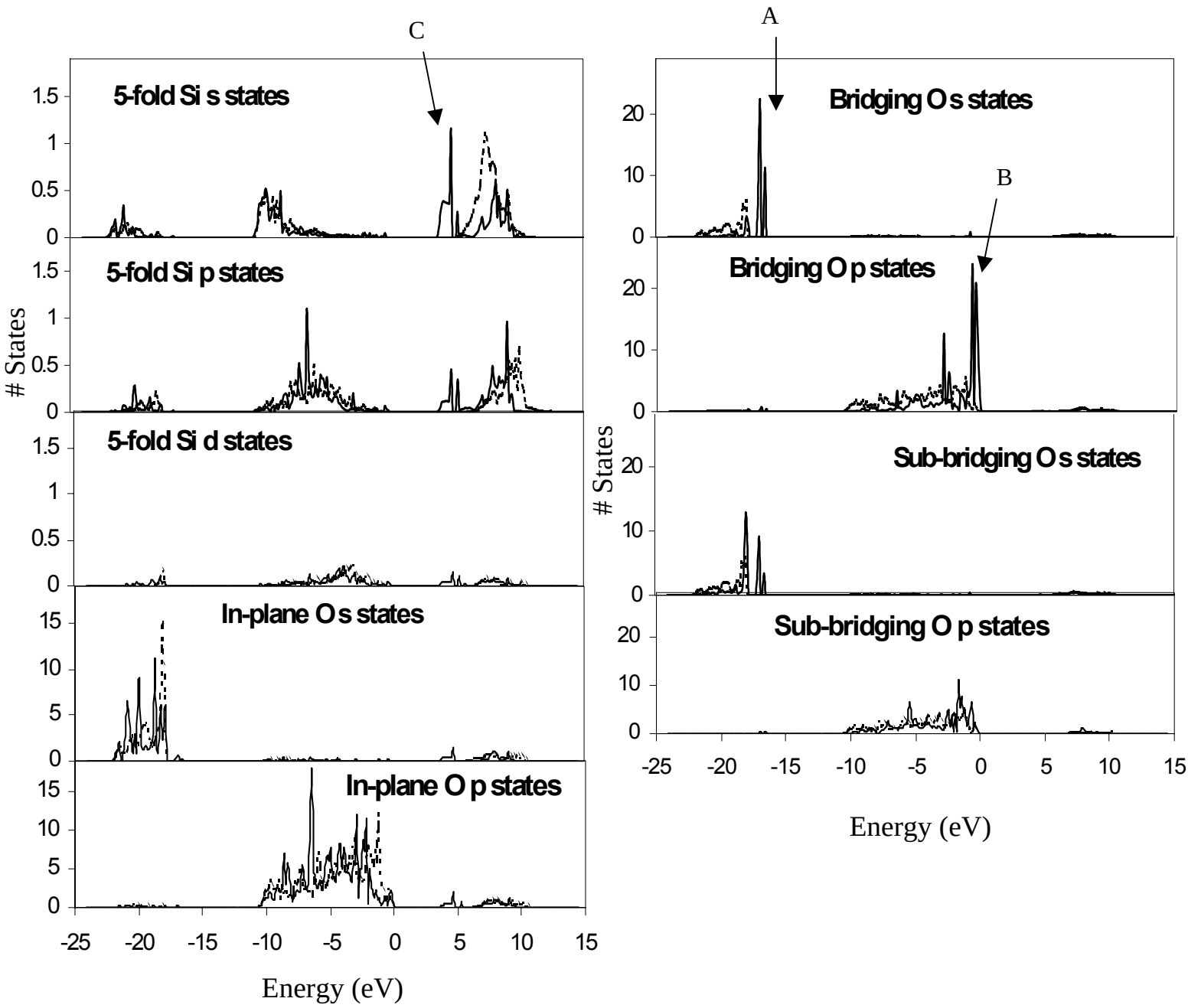

is primarily s in character. The state is localized on specific surface atoms: five-coordinate silicon and in-plane oxygen, with the oxygen and silicon contributions per atom to the state nearly the same (oxygen 8.5% per atom, silicon 7.9%). Again, similar to the bulk PDOS of silicon, the small contributions of surface silicon in the semi-core region can be attributed to the overlap of the spheres centered on the atoms.

2.2.3 Surface Reduction

An approximate electron transfer can be described after consideration of the limitations of electron counting. The total number of electrons counted in the relaxed surface cell is 1.5 less than the number counted in the bulk structure for the same number of atoms. This would lead to a net oxidation of all atoms in the relaxed surface if the electrons were undercounted equally. In this approximation, a reduction of an atom can be considered a true reduction, while an oxidation must be viewed with much more scrutiny. Under these restrictions, it can be seen from the atomic charges that the five- and six- coordinate silicon and the oxygen below the five-coordinate silicon are only slightly reduced relative to the bulk by 0.01, 0.02, and 0.03 electrons, respectively.

2.2.4 ELF and Charge Density Maps

The ELF pictures in Figure 2.7 show how the in-plane and bridging oxygen electronic structure changes with the formation of a surface. The bridging oxygen now shows a banana-shaped lone pair feature across the apex of the Si-O-Si bond. The banana-shaped feature does not separate as the ELF value is increased, which has been

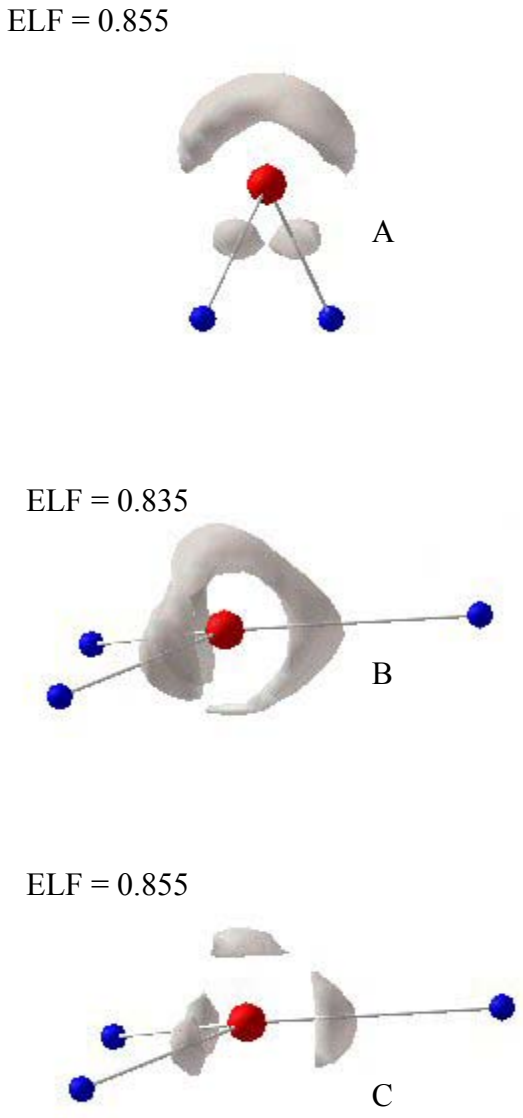

Figure 2.7. (a): Bridging oxygen ELF = 0.855. (b): In-plane oxygen ELF = 0.835. (c): In-plane oxygen ELF = 0.855. The large red spheres are oxygen, the small blue spheres are silicon. The bridging oxygen has both bonding features and a banana-shaped lone pair feature perpendicular to the plane of the Si-O bonds. The in-plane oxygen has asymmetric features at lower values, while increasing the ELF reveals a lone pair feature extending into the vacuum.

seen for various Si-O bonds [22]. The in-plane oxygen shows the same bonding pair features seen in the bulk and features above and below the oxygen at an ELF value of 0.835. The primary difference between the bulk and surface in-plane oxygen is seen when the ELF is increased to 0.855, when the feature below the oxygen (toward the bulk) disappears, leaving only the one lone pair-like feature extending into the vacuum. This change indicates a more localized lone pair extending into the vacuum. The interior oxygen atoms retain essentially bulk characteristics.

The valence charge density isosurfaces also show similar features characteristic of lone pairs. Figure 2.8 shows two different isosurfaces (6.84 and 7.15 $e^-/Å^3$) for both the bridging and in-plane oxygen atoms. The 6.84 $e^-/Å^3$ isosurface for the in-plane oxygen is asymmetric with the isosurface shifted toward the 6-fold silicon and a larger feature on the vacuum side of the oxygen. As the charge density is increased to 7.15 $e^-/Å^3$, the feature below the plane disappears, similar to what is observed with the ELF. The bridging oxygen has symmetric, banana-shaped features for both isosurfaces.

2.3 Molecular Analogs

For the relaxed surface, the electronic structure of the two types of surface oxygen atoms can be seen in terms of molecular analogs: water and H_3O^+. In these two molecular environments, the distribution of charge around the anion controls the geometry.

Figure 2.9 shows three different molecular environments for oxygen: water, planar H_3O^+ and geometry-optimized H_3O^+. The planar H_3O^+ was relaxed only in the plane of the molecule, while the relaxed H_3O^+ molecule was relaxed in three directions.

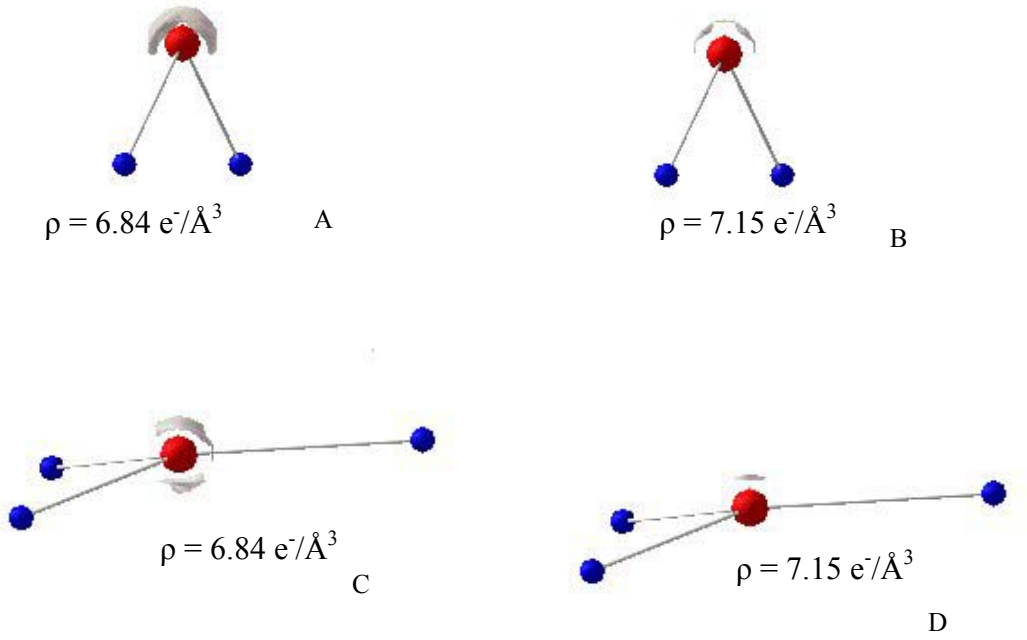

Figure 2.8. Charge density isosurfaces for bridging oxygen and in-plane oxygen. The large red spheres are oxygen, the small blue spheres are silicon. (a) is a charge density isosurface (6.84 $e^-/Å^3$) around a bridging oxygen. (b) shows a different isosurface (7.15 $e^-/Å^3$) surrounding the same atom. (c) is an isosurface (6.84 $e^-/Å^3$) around an in-plane oxygen. (d) is a different isosurface (7.15 $e^-/Å^3$) around the same atom. For the bridging oxygen, the charge density is a symmetric, banana-shaped feature perpendicular to the bond plane. The in-plane oxygen shows an asymmetric charge density distribution at the smaller value, which becomes a lone-pair type feature at the higher value.

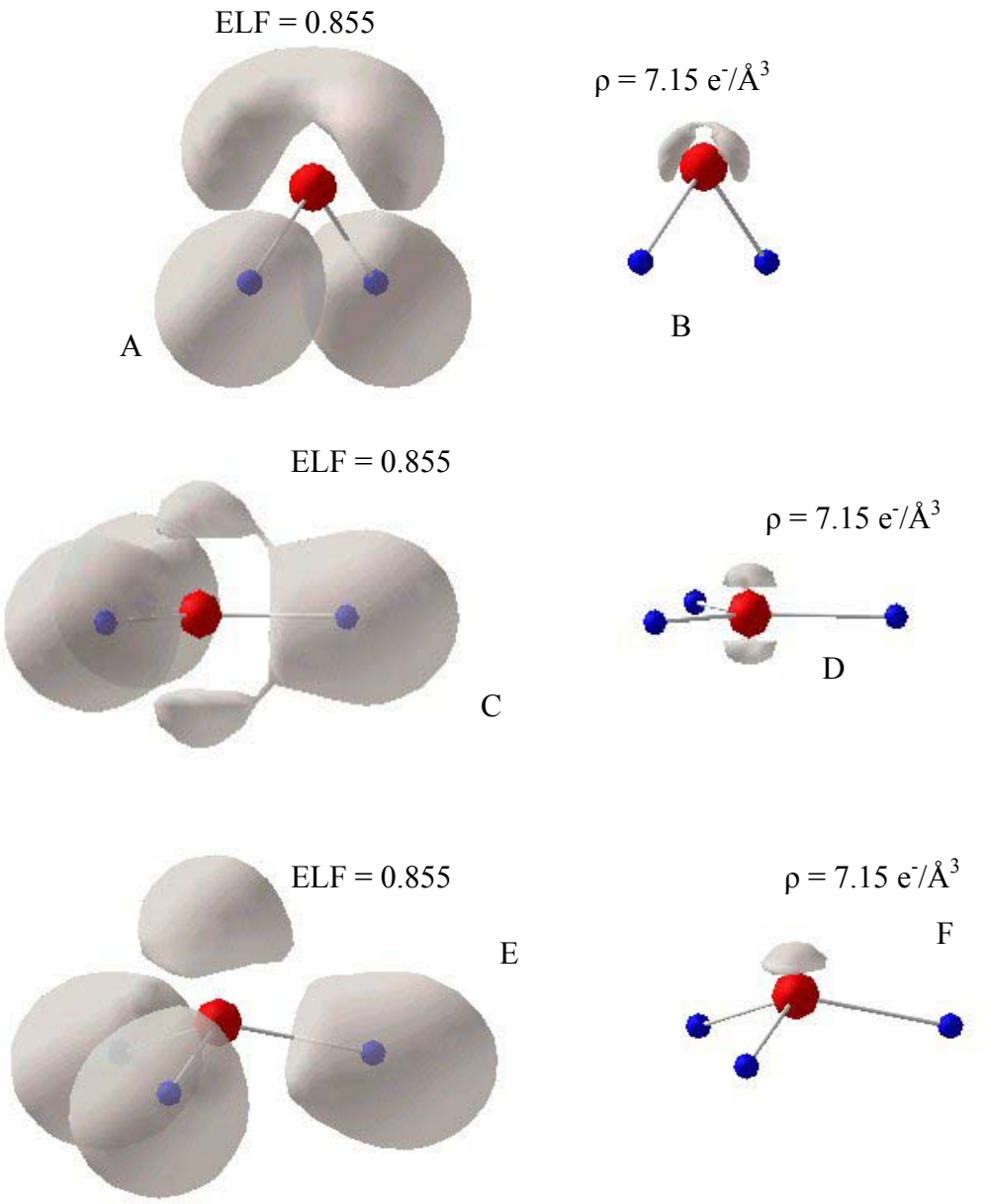

Figure 2.9. The ELF and charge density isosurfaces for (top) water, (middle) planar H_3O^+, and (bottom) relaxed H_3O^+. The large red spheres are oxygen, the small blue spheres are hydrogen. (a): ELF = 0.855 for water molecule. (b) shows a charge density isosurface (7.15 $e^-/Å^3$) for water. (c): ELF = 0.855 for planar H_3O^+. (d) is a charge density isosurface (7.15 $e^-/Å^3$) for planar H_3O^+. (e): ELF = 0.855 for relaxed H_3O^+. (f) is a charge density isosurface (7.15 $e^-/Å^3$) for relaxed H_3O^+. The same lone pair features seen in Figures 7 and 8 for the bridging oxygen are seen for water. The same lone pair features seen in Figure 3 for the bulk oxygen are seen for planar H_3O^+. The same lone pair feature seen in Figures 7 and 8 for the in-plane oxygen is seen for relaxed H_3O^+.

The banana shaped lone pair features across the apex of the H-O-H bond is seen for the ELF = 0.855 value for the water molecule. The same lone pair features are found in the charge density isosurface (7.15 $e^-/Å^3$) for water. The planar H_3O^+ molecule has lone pair features above and below the bonding plane that is seen in the charge density isosurface (7.15 $e^-/Å^3$) and for an ELF value of 0.855. When the molecule is allowed to relax out of the bonding plane, an isolated lone pair feature extending into the vacuum is seen in the charge density isosurface (7.15 $e^-/Å^3$) and for an ELF value of 0.855. The relaxation involves a change from an sp^2 hybridization to an sp^3 hybridization for the oxygen. This forces a change from a trigonal planar to tetrahedral geometry.

A comparison of the ELF and charge density isosurfaces of the surface oxygen atoms to the molecular analogs found in Figure 2.9 reveals the similarity of the oxygen environments. The in-plane oxygen is similar to that of the oxygen in relaxed H_3O^+. The bridging oxygen is in an environment similar to that of oxygen in water. The lone pair features in the ELF and charge density isosurfaces for the in-plane oxygen in Figures 2.7 and 2.8 are seen in Figure 2.9 in the relaxed H_3O^+ molecule. The lone pair features of the bulk oxygen in Figure 2.3 resemble those of the planar H_3O^+ molecule seen in Figure 2.9. The lone pair feature seen in the ELF and charge density isosurfaces for the bridging oxygen in Figures 2.7 and 2.8 are seen in Figure 2.9 in the water molecule.

It appears that without the restrictions of the bulk structure surrounding the surface oxygen atoms, the oxygen atoms exposed to the vacuum adopt a more molecular geometry and electronic structure. Similar to the molecular analogs, the distribution of charge around the oxygen controls the geometry of the relaxed surface. The in-plane oxygen appears to change from an sp^2 hybridization in the bulk, to a more sp^3-like

hybridization on the surface. This change in hybridization state is the same description that has been used to describe in-plane oxygen atoms in SnO_2 [8]. The specific geometric changes can be described using the basic VSEPR model [25]. The sp^3 hybridization in the VSEPR model has a tetrahedral geometry, similar to the observed geometry for in-plane oxygen following surface relaxation with the lone pair extending into the vacuum. The relaxations of the in-plane oxygen out of the surface and five-fold silicon into the surface have been seen for TiO_2 [4] and SnO_2 [5-8]. These relaxations are indicative of the change in the hybridization of the in-plane oxygen and an attempt to assume the new geometry suggested by the VSEPR model. The bridging oxygen also re-hybridizes to sp^3 and adopts a VSEPR geometry, with lone pair features directed perpendicular to the bonding plane. The Si-O-Si angle (109.0°) is nearer to the bond angle suggested by the VSEPR model.

2.4 Conclusions

The DOS for bulk stishovite and the nonpolar stoichiometric (110) surface have been obtained. The bulk DOS compare well with other bulk DOS calculations and the DOS for the surface show the same general characteristics seen by other rutile (110) surface calculations. The relaxation of the surface agrees with other rutile (110) surfaces. Examination of the ELF and charge density lead to the analogy of surface oxygen atoms with the oxygen atoms in H_2O and H_3O^+. Understanding these molecular geometries in simple VSEPR terms can help explain the change in surface oxygen electronic and geometric structure.

Chapter 3 - Hydrogen Fluoride Adsorption

3.1 (110) Surface Adsorption

Adsorption has been studied on the (110) surfaces of rutile structure type oxides for water (TiO_2 [26,27] and SnO_2 [27]), methanol (SnO_2 [28]) and formic acid (TiO_2 [29]). There have been several studies of the bulk electronic structure of stishovite [30-33], and the (110) surface of stishovite has been described in Chapter 2.

For the adsorption of hydrogen fluoride, a Brønsted acid, on oxide surfaces, a cleavage of the H-F bond gives an acidic proton and conjugate base fluoride ion. For a metal-oxygen site pair on the surface, the acidic proton is expected to bind to the basic surface oxygen anion, while the conjugate fluoride ion is expected to bind to a surface metal cation [34,35]. Stishovite is unique in that of all the silica polymorphs, it is the most insoluble in hydrogen fluoride. Studying the adsorption of hydrogen fluoride on the (110) surface may lead to an understanding of the difference between stishovite and other silica polymorphs.

3.2 Hydrogen Fluoride

The equilibrium geometric and electronic structure of molecular hydrogen fluoride was calculated. Due to the use of periodic boundary conditions, the calculations were performed on a periodic array of molecules. To limit interaction between the repeated molecules, the molecule was placed in a cell with the same size of the surface supercell (5.944 Å x 21.889 Å x 5.484 Å). The calculated bond length of 0.938 Å is within 2.3% of the experimental value of 0.917 Å [36].

3.3 Surface Adsorption

Examination of the nonpolar stoichiometric (110) surface yields three types of atomic surface sites where adsorption can occur: 5-fold silicon (one coordination vacancy), in-plane oxygen, and bridging oxygen. The labeled atoms in the relaxed surface described in Chapter 2 are shown in Figure 3.1. The charge density isosurfaces of the surface oxygen atoms shown in Figure 3.2 display details for adsorption sites from calculations of the stishovite (110) surface described in Chapter 2. The bridging oxygen charge density shows a banana-shaped isosurface perpendicular to the Si-O bonding plane. The bridging oxygen ELF shown in Figure 3.2 reveals the same characteristics, but also shows bonding pairs along the Si-O bonds. The coordination and lone pair electronic structure of the bridging oxygen is similar to the oxygen in water, and the localized electron density in this lone-pair can be used to bond hydrogen. The in-plane oxygen charge density shows a lone-pair feature on the in-plane oxygen extending into the vacuum that can also be a site for hydrogen adsorption. The in-plane oxygen ELF exhibits the same characteristics, along with the bonding pairs along the Si-O bonds. The coordination and lone pair electronic structure of the in-plane oxygen is similar to the oxygen in molecular H_3O^+.

Individual hydrogen and fluorine adatoms, hydrogen and fluorine adatom pairs (predissociated molecular HF), and molecular hydrogen fluoride adsorptions have been

Figure 3.1. The relaxed nonpolar stoichiometric (110) surface of stishovite. Large red spheres are oxygen atoms, small blue spheres are silicon atoms.

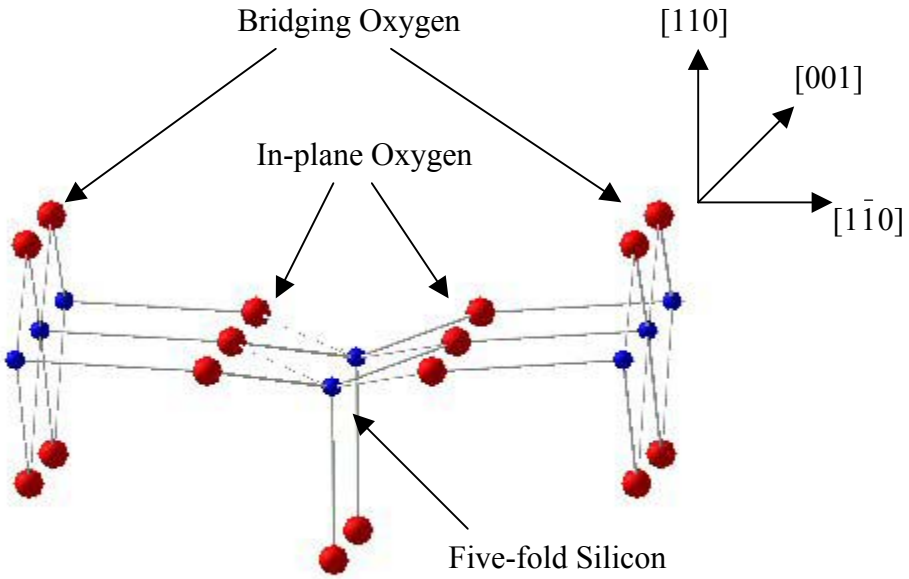

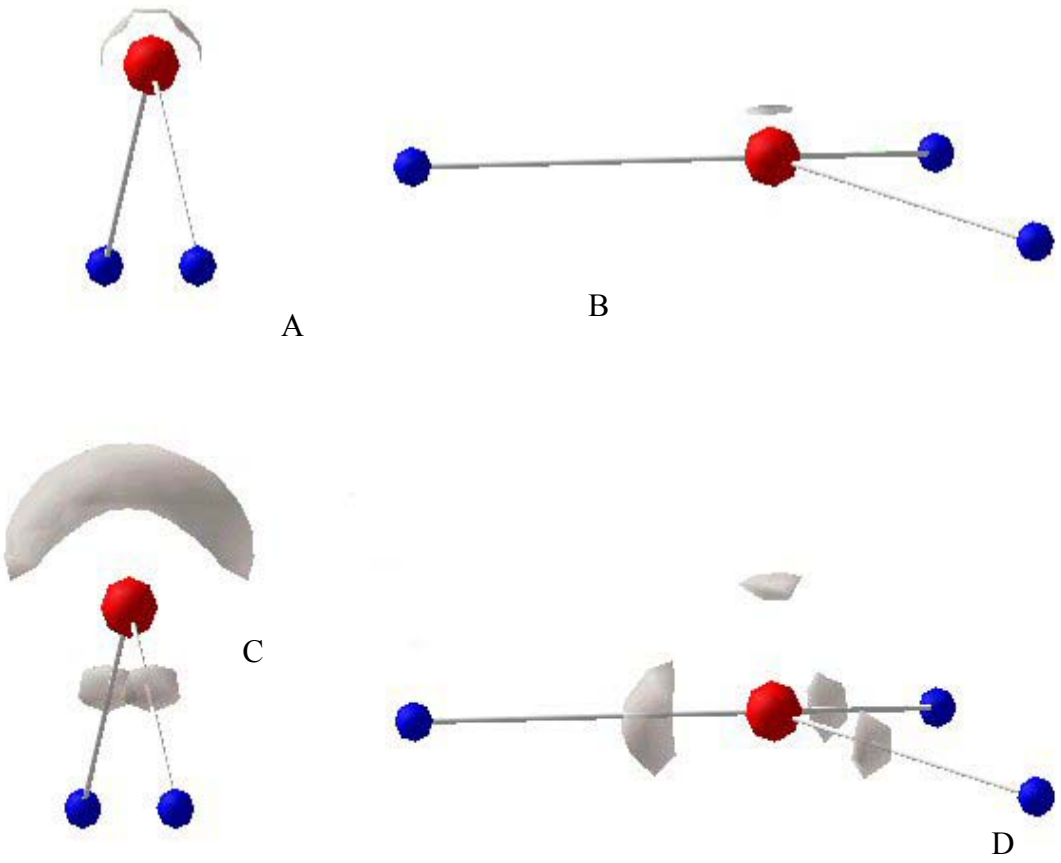

Figure 3.2. Charge density isosurfaces ($7.15e^{-}/ Å^{3}$) for (a) bridging oxygen and (b) in-plane oxygen. ELF=0.86 for the (c) bridging and (d) in-plane oxygen. Small blue spheres represent silicon atoms, large red spheres represent oxygen atoms. The lone pair feature across the apex of the Si-O-Si bond can be seen in both the ELF and charge density for bridging oxygen. The lone pair feature extending into the vacuum can be seen in both the ELF and charge density for in-plane oxygen. The ELF shows bonding pair features along Si-O bond vectors.

studied at these sites. A positive adsorption energy indicates a decrease in the total energy of the system after adsorption occurs. The forces on all atoms were less than 0.35 eV/Å in all adsorption calculations.

3.3.1 Individual Adatom Adsorption

Individual fluorine and hydrogen adatoms were placed alone on the surface at specific surface atoms. A fluorine adatom was placed over the five-fold silicon. A hydrogen adatom was placed at the five-fold silicon, the in-plane oxygen, and the bridging oxygen. The final structures for hydrogen adatom adsorption are seen in Figure 3.3. The adsorption energies are listed in Table 3.1. The hydrogen adatom adsorption on the bridging oxygen site is the most favored energetically, while the in-plane oxygen site is the least favored.

3.3.1.1 Bridging Oxygen Hydrogen Adsorption

The final location of the hydrogen on bridging oxygen seen in Figure 3.3 is not vertical, but tilted in the $[1\bar{1}0]$ direction. This location is, however, dependent on the parameters for the calculation. There is a shallow local minimum in the potential curve corresponding to slight changes in tilt angle, so the degree of tilting is strongly dependent on the convergence criteria. The O-H bond length is 0.98 Å.

For hydrogen adatom adsorption on bridging oxygen, displacements are seen for all the surface atoms relative to the clean surface. The six-fold silicon atoms displace into the surface 0.14 Å. The five-fold silicon in the same $[1\bar{1}0]$ direction row displaces out of the surface 0.15 Å, while the other 5-fold silicon displaces slightly (0.04 Å) into the surface.

The in-plane oxygen atoms nearest the hydrogen displace into the surface (0.07 Å), while the in-plane oxygen atoms further away displace less (0.05 Å) into the surface. The Si-O bond for the oxygen with adsorbed hydrogen increases to 1.82 Å, compared to the neighboring bridging oxygen Si-O bond lengths of 1.69 Å.

The ELF and charge density isosurfaces for the bridging oxygen adsorption site are seen in Figure 3.4. As the ELF is increased to a value of 0.86, a lone pair feature is seen on the side opposite of hydrogen. A related feature is also seen in the charge density maps. The geometry and lone pair features of this three-coordinate oxygen resemble the in-plane oxygen of the relaxed surface shown in Figure 3.2.

3.3.1.2 In-plane Oxygen Hydrogen Adsorption

The hydrogen adatom adsorption on the in-plane oxygen creates surface displacements larger than 0.1 Å in both the [110] and [$1\bar{1}0$] directions. All displacements are larger than those for the hydrogen adsorption on the bridging oxygen site. The overall effect of these displacements is to produce large bond length and angle variations compared to the clean surface. The O-H bond length (1.00 Å) is also slightly larger in comparison.

The ELF (Figure 3.5) bonding pair features of the in-plane oxygen adsorption site resemble those of the clean site, but the lone pair feature is replaced by hydrogen. Additionally, one five-fold silicon displaces out of the surface and the other displaces into the surface, relative to the clean surface. The five-fold silicon that displaces out of the

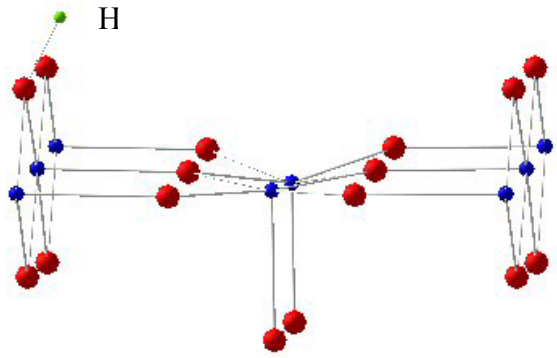

A

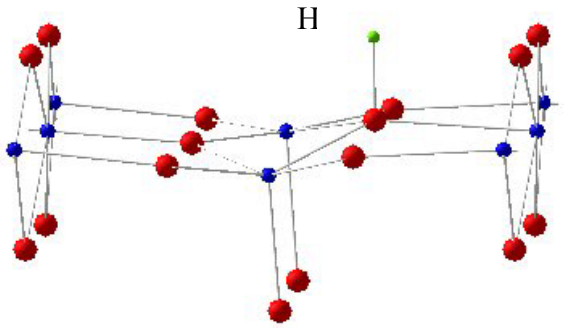

B

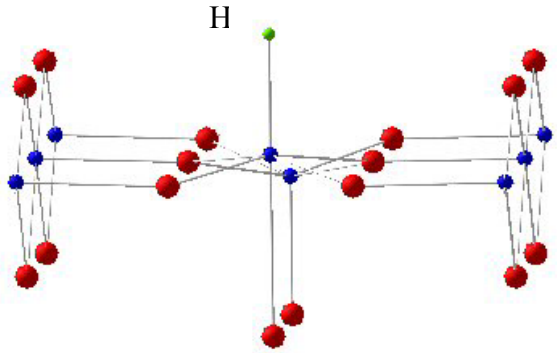

C

Figure 3.3. Relaxed structures of hydrogen adatom adsorption. (a) Bridging oxygen adsorption site (b) In-plane oxygen adsorption site (c) Silicon adsorption site. The surface atoms are represented the same as in Figure 1 (Large red spheres are oxygen atoms, small blue spheres are silicon atoms), while the adsorbed hydrogen is represented by small green spheres.

Adsorption Site	Hydrogen Adatom Adsorption Energy (kJ/mol)
In-plane Oxygen	24.8
Bridging Oxygen	172.1
Silicon	115.6

Table 3.1. Hydrogen adatom adsorption energies for selected adsorption sites.

surface has a large feature that resembles a lone pair extending into the vacuum. This silicon is reduced by 0.06 electrons compared to the relaxed surface. The feature is isolated on that silicon, even when the cell dimension is doubled in the [001] direction (to features indicate the hydrogen adsorption induces a dangling bond state on the neighboring silicon. Interestingly, though, the charge density ($0.15e^-/Å^3$) isosurface features on that silicon do not appear any different than the features of any other silicon.

3.3.1.3 5-Fold Silicon Adsorption Site

The fluorine and hydrogen adatom adsorptions on the five-fold silicon site have a similar effect on the surface, with the only difference being the displacement of the silicon adsorption site. For the fluorine adatom adsorption, the silicon displaces out of the surface 0.41 Å, while for the hydrogen adatom adsorption, the displacement is 0.51 Å. These displacements increase the silicon – in-plane oxygen bond length to avoid interaction with adsorbed hydrogen in the neighboring repeated cell). The ELF 1.82 Å a 2.5% increase from the clean surface. The Si-F bond length is 1.61 Å, while the Si-H bond length is 1.47 Å. The fluorine adatom adsorption energy (320.8 kJ/mol) is larger than the hydrogen adatom adsorption energy (115.6 kJ/mol), which follows from the larger bond enthalpy for Si-F.

3.3.2 Hydrogen and Fluorine Adatom Co-adsorption

Fluorine and hydrogen adatom pairs (pre-dissociated) were placed onto the relaxed surface in two distinct starting positions, one with the hydrogen on an in-plane oxygen (HIF) and one with the hydrogen on a bridging oxygen (HBF). In both cases

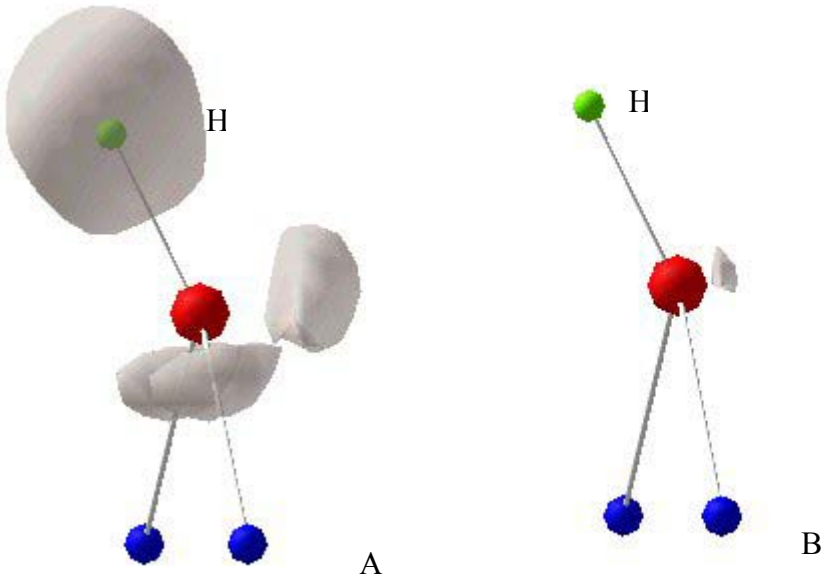

Figure 3.4. (a) ELF = 0.86 and (b) charge density ($7.32e^{-}/Å^{3}$) isosurfaces for the bridging oxygen adsorption site. The small blue spheres are silicon atoms, the large red spheres are oxygen atoms. The smaller green sphere represents hydrogen.

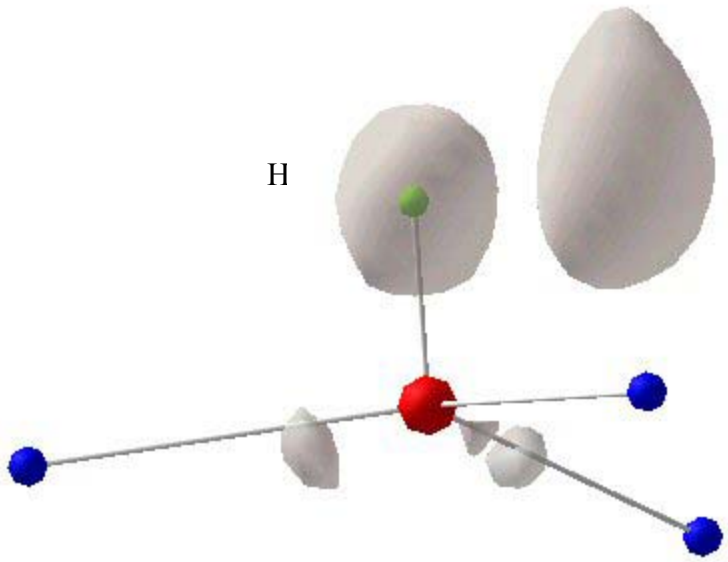

Figure 3.5. ELF = 0.87 isosurface for the in-plane oxygen with hydrogen adatom adsorption. The small blue spheres are silicon atoms, the large red spheres are oxygen atoms. The smaller green sphere represents hydrogen.

the fluorine adatom was placed over the 5-fold silicon. The relaxed structures are seen in Figure 3.6 and the adsorption energies are listed in Table 3.2. The adsorption energy was calculated using an initial state of molecular hydrogen fluoride for consistency, even though there was no formal HF bond. As seen for individual adatom adsorption, the bridging oxygen adsorption site is energetically preferred for hydrogen adatom binding. The difference in adatom pair (HBF and HIF) adsorption energy almost matches the difference in adsorption energy for hydrogen adatom adsorption energy for the in-plane and bridging oxygen sites.

3.3.2.1 Hydrogen/Silicon Adatom Pair – Bridging Oxygen Adsorption Site

The relaxed HBF geometry has a combination of the features of fluorine adatom adsorption and hydrogen adatom adsorption on the bridging oxygen site. Similar to the hydrogen adatom adsorption, the six-fold silicon displace into the surface 0.12 Å and the in-plane oxygen atoms displace into the surface 0.09 Å. Similar to the fluorine adatom adsorption, the silicon adsorption site displaces out of the surface by 0.30 Å. The Si-F (1.68 Å) and O-H (0.98 Å) bond lengths are similar to those seen for their respective adatom adsorption. The hydrogen and fluoride are tilted toward each other and are separated by 2.26 Å.

The adsorbed fluorine has no effect on the bridging oxygen adsorption site, as the ELF and charge density isosurfaces display the exact same details seen for hydrogen adatom adsorption when the fluorine adatom was not present.

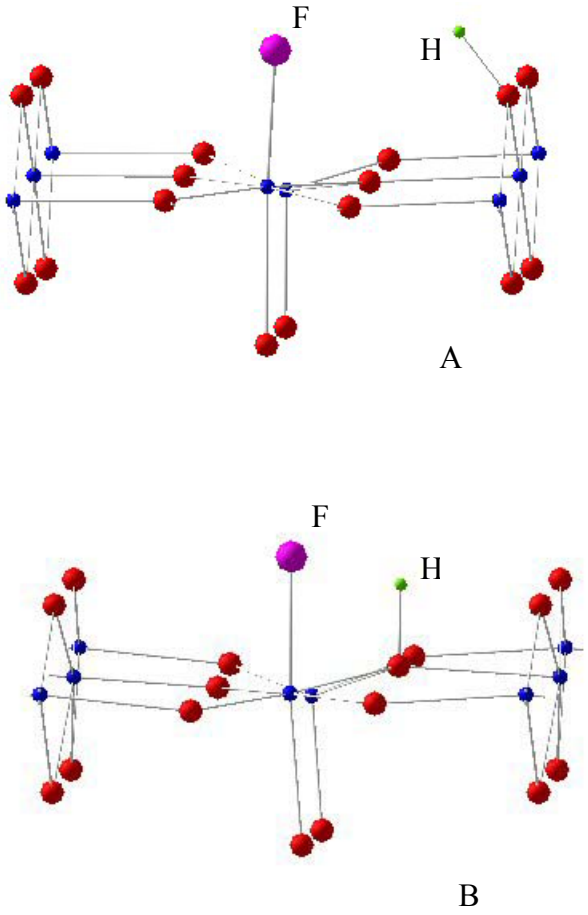

Figure 3.6. Relaxed structures of (a) HBF and (b) HIF adatom pair adsorption. The small blue spheres are silicon atoms, the large red spheres are oxygen atoms. The smaller green sphere represents hydrogen and the larger purple sphere represents fluorine.

Adsorption Geometry	Adsorption Energy (kJ/mol)
H and F adatom pair – hydrogen on in-plane oxygen	10.4
H and F adatom pair – hydrogen on bridging oxygen	176.4
HF molecular dissociation	177.8
Overall average (HBF and HF dissociation)	177.3
HF molecular physisorption	34.5

Table 3.2. Adsorption energies for adatom pairs and molecular adsorption. The value for HF molecular dissociation is an average of the two different starting positions that give dissociation.

3.3.2.2 Hydrogen/Silicon Adatom Pair – In-plane Oxygen Adsorption Site

The relaxed HIF geometry has a combination of the features of fluorine adatom adsorption and hydrogen adatom adsorption on the in-plane oxygen site. The Si-F bond length is 1.67 Å and the in-plane O-H bond length is 1.00 Å. The fluorine adatom is tilted toward the hydrogen, with an H-F distance of 1.89 Å. Large surface displacements (>0.1 Å) are seen similar to those for the hydrogen adatom adsorption on in-plane oxygen, while the same displacement (0.26 Å) out of the surface is seen for the silicon adsorption site.

As a result of the displacements, the bond lengths change greatly between the in-plane oxygen atoms and the surface silicon atoms. The bond lengths between the in-plane oxygen and its nearest neighbor silicon atoms all increase compared to the clean surface: the five-fold silicon bond distance is 1.86 Å (4.5% increase), the six-fold silicon bond length is 1.98 Å (5.1% increase), and the fluorine adatom - silicon bond length is 1.94 Å (9.0% increase).

The ELF and charge density isosurfaces of the in-plane oxygen with adsorbed hydrogen are different in the fact that the lone pair-like feature on silicon is no longer seen. Additionally, the lone pair feature on the in-plane oxygen is replaced with adsorbed hydrogen.

3.3.3 Molecular HF adsorption

Three distinct initial positions for molecular adsorption, all aligned perpendicular to the surface in the [110] direction, were studied. As shown in Figure 3.7 they are:

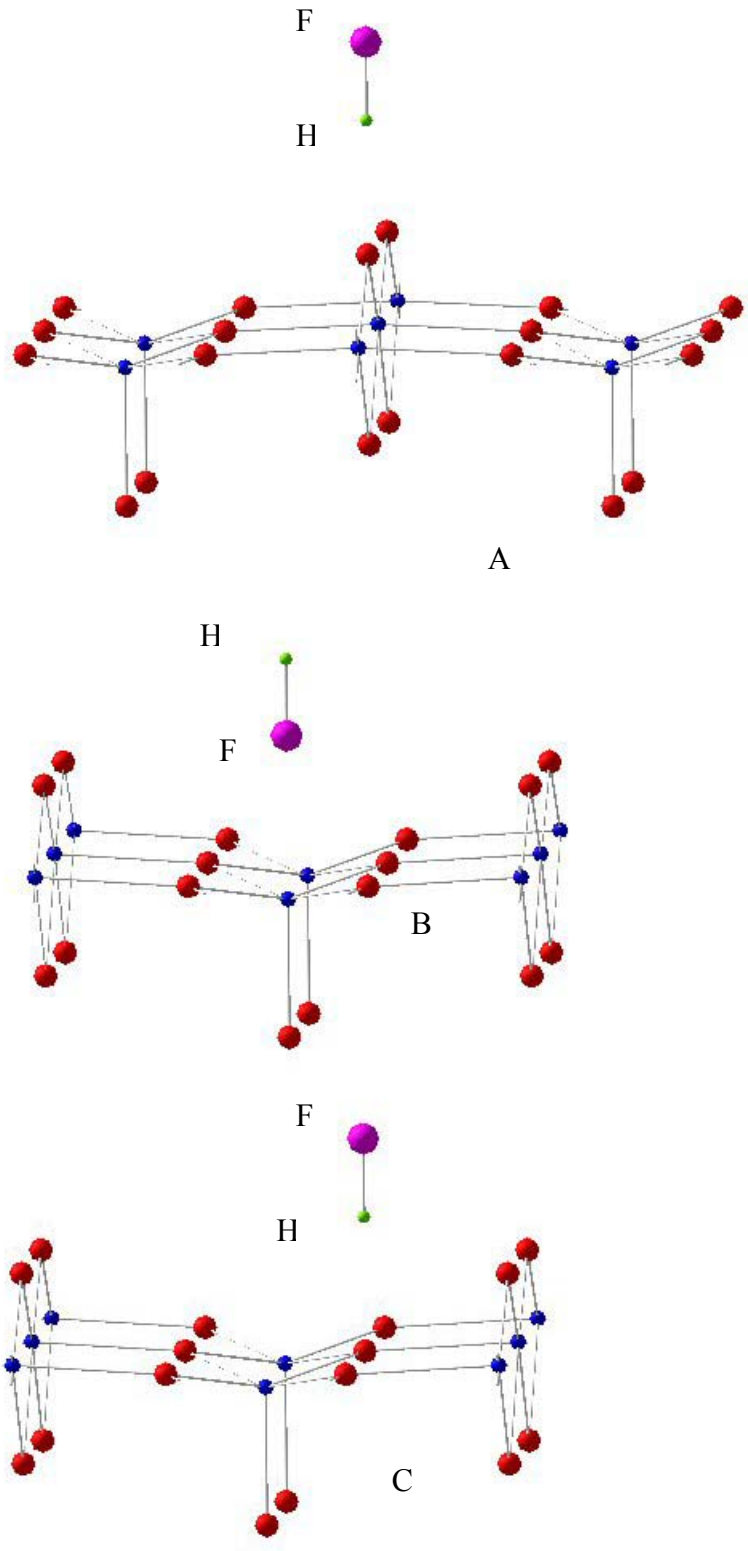

Figure 3.7. Starting structures for molecular adsorption on (a) bridging oxygen site, (b) silicon site, and (c) in-plane oxygen site. The small blue spheres are silicon atoms, the large red spheres are oxygen atoms. The smaller green sphere represents hydrogen and the larger purple sphere represents fluorine.

hydrogen end down on an in-plane oxygen adsorption site, fluoride end down over a silicon adsorption site, and hydrogen end down on a bridging oxygen adsorption site.

3.3.3.1 Molecular Adsorption – In-plane Oxygen and 5-Fold Silicon

The relaxed structures for hydrogen fluoride at the in-plane oxygen and silicon sites give dissociated HF upon geometry optimization, with the fluorine bonded to the silicon site and the hydrogen bonded to the bridging oxygen site. These essentially match the HBF optimized geometry seen in Figure 3.6. The average optimized bond lengths and displacements for both molecular dissociations match the values for the HBF geometry. All three structures lie in the shallow local minimum corresponding to essentially the same geometry. Table 3.2 lists the average adsorption energy for both structures, which also match the HBF adsorption. The lone pair features in the ELF and charge density isosurfaces are very similar to those seen in Figure 3.4 for separate adatom adsorption.

3.3.3.2 Molecular Adsorption – Bridging Oxygen

The case of molecular hydrogen fluoride adsorption aligned vertically (hydrogen end down) over a bridging oxygen produced a favorable adsorption energy of 34.5 kJ/mol, which compares well to a calculation of a hydrogen fluoride/water system, where the hydrogen bonding energy was 31.5 kJ/mol [37].

The relaxed structure is a local minimum very similar to the initial geometry. The alignment of the HF molecule is vertical above the bridging oxygen with no tilt of the molecule, evidenced by the O-H-F bond angle of 180.0°. The surface structure changes only slightly, with the largest changes from the clean relaxed surface being the relaxation

of the 6-fold silicon and bridging oxygen atoms into the surface by 0.03 Å. The bond length between the bridging oxygen and the hydrogen is 1.641 Å. This bond length compares favorably to calculations by Grabowski [37] for the HF/H_2O system with an $FH\text{-}OH_2$ bond length of 1.730 Å. The H-F bond also stretches by 2.1% to 0.958 Å, which agrees well with the 1.6% increase in length seen in the HF/H_2O system [37].

A minor change in oxygen electronic structure can be seen through examination of the ELF and charge density isosurfaces shown in Figure 3.8. Molecular HF is included in Figure 3.8 for comparison. The ELF value of 0.86 (Figure 3.8a) of the bridging oxygen adsorption site shows the same features seen for the same atom at the clean surface, namely the banana-shaped lone pair across the apex of the Si-O-Si bond and the bonding pairs directed along the Si-O bonds. However, as the ELF is increased to 0.875 (Figure 3.8b), the lone pair feature disappears at the bridging oxygen adsorption site before the clean bridging oxygen. The features of the charge density isosurfaces (Figure 3.8c) for the adsorbed and clean bridging oxygen sites match very well qualitatively. The only difference is the charge density for the bridging oxygen adsorption site separates into two distinct lone pair features for the same charge density where only one feature is seen on the clean site. The properties suggest a physisorbed HF that is a possible molecular precursor to dissociation.

3.4 Bonding in HF adsorption

In all cases studied, the dissociative adsorption of hydrogen fluoride is energetically favored. There is, however, a clear energetic preference of hydrogen binding at a bridging oxygen site. This proton – base site combination causes smaller

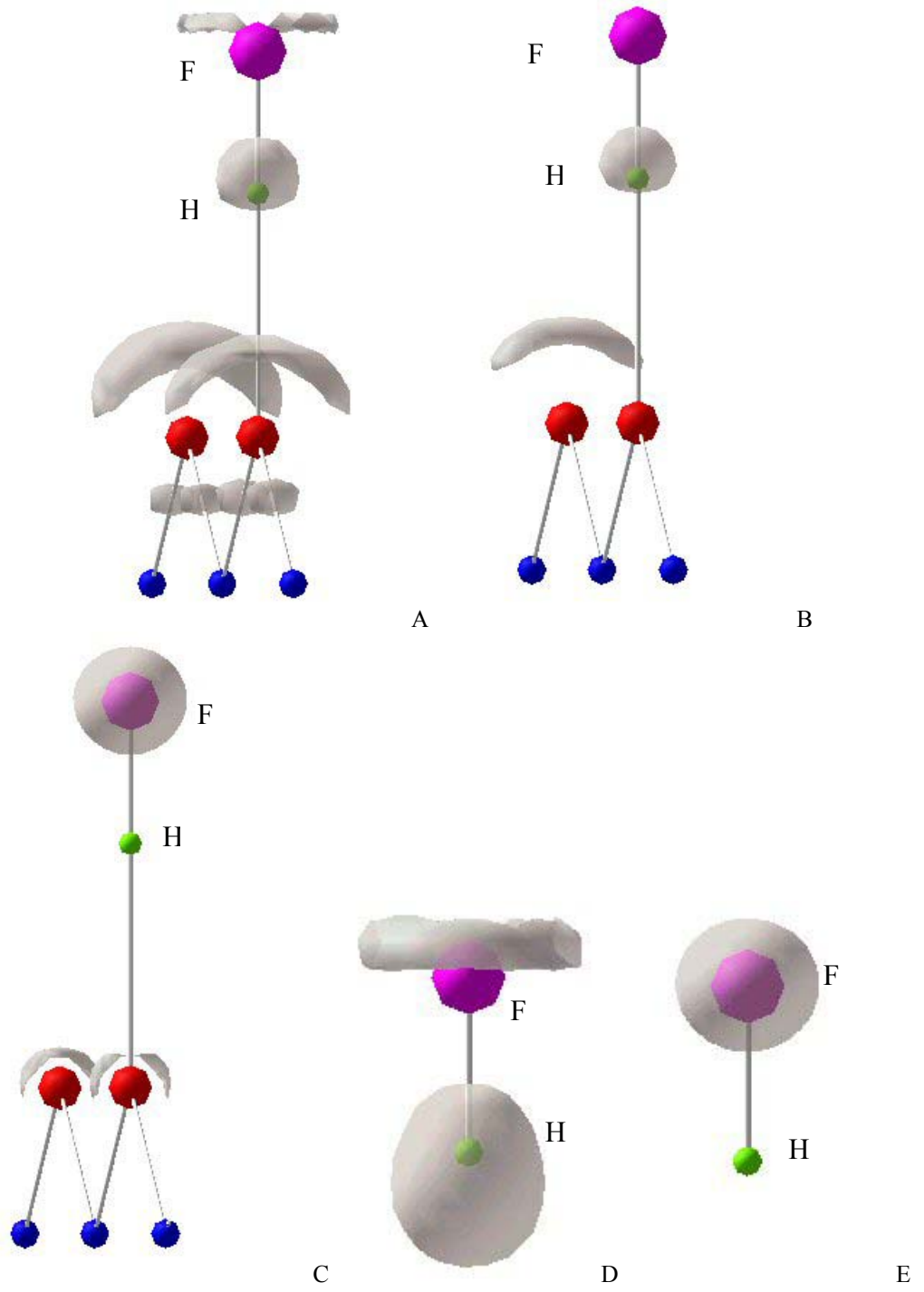

Figure 3.8. (a) ELF = 0.86 (b) ELF = 0.875 and (c) Charge density ($7.01e^-/Å^3$) isosurfaces for the bridging oxygen adsorption site and nearest clean site for molecular HF adsorption. The (d) ELF = 0.86 and (e) charge density ($7.01e^-/Å^3$) isosurface of the HF molecule are included for comparison. The small blue spheres are silicon atoms, the large red spheres are oxygen atoms. The smaller green sphere represents hydrogen and the larger purple sphere represents fluorine.

displacements in the surface compared to proton binding to the in-plane oxygen adsorption site.

The stereochemical lone pairs on the clean bridging oxygen site are the coordination locations for hydrogen adatom binding. The lone pairs change when adsorption occurs. Upon adsorption, the bridging oxygen changes in oxygen environment from Si_2O to Si_2OH. The difference in oxygen environment is similar to that of bridging (two lone pairs) and in-plane oxygen (one lone pair) sites on the clean surface, whose local coordination and electronic properties resemble their molecular analogs: H_2O and H_3O^+, respectively. This can be seen in the ELF and charge density isosurfaces, where after the adsorption of hydrogen at the bridging oxygen site, the oxygen resembles an in-plane oxygen in the relaxed surface. The same tilt in the $[1\bar{1}0]$ direction characteristic of a H_3O^+-like molecular environment is seen for the binding of a proton to a surface bridging oxygen in the dissociative adsorption of water on both TiO_2 and SnO_2 (110) surfaces [27]. Additionally, the energy profile around the bridging oxygen has a shallow local minimum, which accounts for the slight discrepancy in the final geometry of similar structures.

The in-plane oxygen site has only one lone pair coordination site for hydrogen atoms. The Si_3O environment of the in-plane oxygen is an H_3O^+-like environment. The lone pair extends into the vacuum and the geometry is a distorted tetrahedron. Additional adsorption at the lone-pair requires a change in the geometry of the oxygen site. This relaxation is restricted due to the presence of the bulk. Adsorption at this site causes large (>0.1 Å) displacements in surface atoms, which greatly increases the energy of the system.

3.5 Conclusions

The adsorption of hydrogen fluoride is energetically favored in all cases studied. The proton has an energetic preference for the bridging oxygen adsorption site, which undergoes a change in oxygen environment to accommodate additional coordination. There is a shallow local minimum for adsorption structures, which account for slightly different geometries for the same net adsorption. A physisorbed molecular precursor to dissociation was found at the bridging oxygen adsorption site.

Chapter 4 - Conclusions

4.1 Overall Conclusions

The density of states and geometry for bulk stishovite and the (110) surface have been obtained and compare well with previous calculations for both stishovite and other rutile (110) surfaces. Examination of the ELF and charge density maps of surface oxygen atoms (both bridging and in-plane) lead to comparisons with oxygen atoms in similar molecular environments. The bridging oxygen surface atom resembles oxygen in molecular H_2O, while the in-plane oxygen resembles the oxygen in molecular H_3O^+. These molecular analogs can be described using the simple VSEPR model, and extending the comparison to the surface oxygen atoms helps to describe the change in electronic and geometric structure. The use of the molecular VSEPR model can be extended to surface atoms on oxide surfaces, where molecular analogs to surface atoms can be found.

The dissociative adsorption of hydrogen fluoride is energetically favored in all the cases studied. The proton has an energetic preference for the more basic bridging oxygen adsorption site, where there is a range of energetically similar structures (surface-O-H bond angles) due to a shallow potential energy surface controlling the location of the proton on the bridging oxygen. A physisorbed molecular precursor to dissociation was found at the bridging oxygen adsorption site.

4.2 Recommendations for Future Work

The study of the adsorption of molecular hydrogen fluoride produced results that can use further exploration. Specifically, two molecular adsorptions studied give dissociated products. Due to the length of the calculations, the exact energy barrier to

dissociation was not investigated. The Nudged Elastic Band (NEB) technique, which calculates the energy of snapshots along the reaction pathway, could be used to probe the presumably low energy barrier to dissociation. There are also different starting geometries for molecular adsorbates that have not been tried. These include a horizontal position above bridging oxygen, with the fluoride end directed in the $[1\bar{1}0]$ direction, and directed vertically above the five fold silicon, with the hydrogen end down.

A unique aspect of stishovite is its resistance to etching by hydrogen fluoride. A study of hydrogen fluoride adsorption on a quartz surface would provide a background to understand the difference in the Si-O bonding during adsorption in both cases.

Adsorption on oxide surfaces have often been studied using H_2O as the adsorbing species. A better comparison of the adsorption on the (110) surface of stishovite with that of other oxide surfaces can be made using water as the probe molecule.

Finally, the calculations made can be compared to experiments conducted on a single crystal. Stishovite has been synthesized, and, if it is possible, a single crystal for ultrahigh vacuum studies might be obtainable.

References

[1] Stishov, S.M., Popova, S.V., *Geochem*., **10**, 1961, 923.

[2] Chao, E.C., Fahey, J.J., Littler, J., Milton, E., *J. Geophys. Res*., **67**, 1962, 419.

[3] Kirfel, A., Krane, H.-G., Schwarz, K., Lippmann, T., *Acta. Cryst*., **A57**, 2001, 663.

[4] Bates, S.P., Kresse, G., Gillan, M.J., *Surf. Sci*., **385**, 1997, 386.

[5] Oviedo, J., Gillian, M.J., *Surf. Sci*., **463**, 2000, 93.

[6] Manassidis, I., Goniakowski, J., Kantorovich, L.N., Gillan, M.J., *Surf. Sci*., **339**, 1995, 258.

[7] Maki-Jaskari, M.A., Rantala, T.T., *Phys. Rev. B*, **64**, 075407.

[8] Godin, T.J., LaFemina, J.P., *Phys. Rev. B*, **47**, 1993, 6518.

[9] Alvarez, J.R., Rez, P., *Solid State Commun*., **108**, 1998, 37.

[10] Dewhurst, J.K., Lowther, J.E., Madzwara, L.T., *Phys. Rev. B*, **55**, 1997, 11003.

[11] Xu, Y.-N., Ching, W.Y., *Phys. Rev. B*, **44**, 1991, 11048.

[12] Rudra, J.K., Fowler, W.B., *Phys. Rev. B*, **28**, 1983, 1061.

[13] Kresse, G., Hafner, J., *Phys. Rev. B*, **47**, 1993, RC558.

[14] Kresse, G., Furthmüller, J., *Phys. Rev. B*., **54**, 1996, 11169.

[15] Kresse, G., Furthmüller, J., *Comput. Mat. Sci*., **6**, 1996, 15

[16] Vanderbilt, D., *Phys. Rev. B*, **41**, 1990, 7892.

[17] Perdew, J., Chevary, J., Vosko, S., Jackson, K., Pederson, M., Singh, D., Fiolhais, C., *Phys. Rev. B*, **46**, 1992, 6671.

[18] Perdew, J., Wang, Y., *Phys. Rev. B*., **45**, 1992, 13244.

[19] Monkhorst, H., Pack, J., *Phys. Rev. B*., **13**, 1976, 5188.

[20] Becke, A.D., Edgecombe, K.E., *J. Chem. Phys*., **92**, 1990, 5397.

[21] Savin, A., Nesper, R., Wengert, S., Fassler, T.F., *Angew. Chem*., **36**, 1997, 1808.

[22] Gibbs, G.V., Cox, D.F., Boisen Jr., M.B., Downs, R.T., Ross, N.L., *Phys. Chem. Minerals*, **30**, 2003, 305.

[23] Gibbs, G.V., Cox, D.F., Crawford, T.D., Boisen Jr., M.B., Lim, M., *Phys. Chem. Minerals*, **29**, 2002, 307.

[24] Ross, N.L., Shu, J.F., Hazen, R.F., Gasparik, T., *Am. Mineral*., **75**, 1990, 739.

[25] Gillespie, R.J., *Molecular Geometry*, Van Nostrand Reinhold, London, 1972.

[26] Stefanovich, E.V., Truong, T.N., *Chem. Phys. Lett*., **299**, 1999, 623

[27] Goniakowski, J., Gillan, M.J., *Surf. Sci*., **350**, 1996, 145.

[28] Calatayud, M., Andrés, J., Beltrán, A., *Surf. Sci*., **430**, 1999, 213.

[29] Käckell, P., Terakura, K., *Appl. Surf. Sci*., **166**, 2000, 370.

[30] Alvarez, J.R., Rez, P., *Solid State Commun*., **108**, 1998, 37.

[31] Dewhurst, J.K., Lowther, J.E., Madzwara, L.T., *Phys. Rev. B*, **55**, 1997, 11003.

[32] Xu, Y.-N., Ching, W.Y., *Phys. Rev. B*, **44**, 1991, 11048.

[33] Rudra, J.K., Fowler, W.B., *Phys. Rev. B*, **28**, 1983, 1061.

[34] Barteau, M.A., *J. Vac. Sci. Technol. A*, **11**, 1993, 2162.

[35] Barteau, M.A., *Chem. Rev.*, **96**, 1996, 1413.

[36] Huber, K., Herzberg, G., *Molecular Spectra and Molecular Structure*, Van Nostrand, Princeton, 1978.

[37] Grabowski, S.J., *Chem. Phys. Lett*., **338**, 2001, 361.